15TH IEA HEAT PUMP CONFERENCE
MAY 26–29, 2026 | HOFBURG
VIENNA 2026
DECARBONISATION THROUGH INNOVATION

Seasonal performance assessment of large size air-source heat pumps with multiple evaporators affected by frosting and defrosting cycles

A.F. Passarelli[a], F. Pelella[a], L.Viscito[a], U. Merlo[b], S.Filippini[b], A.W. Mauro[a*]

[a] Department of Industrial Engineering, Università degli Studi di Napoli–Federico II, P.le Tecchio 80, 80125 Naples, Italy
[b]Lu-Ve S.p.A., Uboldo, Italy

Abstract

Large-scale heat pumps are considered a mature technology for integration into new district heating networks and for decarbonizing existing ones that currently rely on fossil fuels. Among the available heat sources, air-source heat pumps offer a universally applicable solution. However, in cold and humid climates, frost formation becomes a critical issue, affecting the performance of the multi air-to-refrigerant evaporator system. To ensure uninterrupted service to the district heating network, defrosting of the evaporators must be non-simultaneous, but this necessary operation inevitably impacts overall system performance. This study involves a novel model designed to estimate the seasonal performance of this kind of systems, based on a detailed dynamic model of the evaporator field, capturing the behaviour of each individual heat exchanger, including their frosting and defrosting cycles. The aim of this work is to quantify the impact of frost formation on seasonal efficiency, exploring a domain of 20 evaporator field configurations and 4 time-based defrosting strategy settings for a case study located in Harbin, China. Using total costs as performance parameter, the configurations analysed resulted in a maximum of about 16% difference between the best and worst solutions. Configurations with a wide fin pitch proved to be the most convenient regardless defrosting strategy. Instead, the best defrosting strategy on average was the one with the lowest frequency, due to the low mean ambient temperature and humidity of the location. Nevertheless, it is the combination of field configuration and defrosting strategy to define the proper optimal solution, valid in the chosen case study.

Keywords: Large-size; Air-source; Frosting; Defrosting; Multi-Evaporator; Seasonal performance

1. Introduction

The decarbonization of the heating sector represents one of the main challenges to achieve global climate targets. At the present time, almost half of the global final energy consumption is associated with heat production, and the sector remains heavily dependent on fossil fuels [1]. Electrification through vapor compression heat pumps is widely recognized as one of the most effective strategies to reduce both primary energy consumption and CO_2 emissions.

District heating networks are expected to cover nearly 20% of the heating demand in Europe by 2050, representing a particularly promising field of application for large air-source heat pumps [2]. These systems offer operational flexibility, can be integrated into existing thermal infrastructures, and are suitable to be coupled with renewable electricity production. Typical large-scale installations rely on ammonia as working fluid arranged in two-stage cycles, equipped with screw compressors and extensive evaporator fields made up of fin-and-tube heat exchangers operating in parallel. These kinds of configuration allow high heating

* Corresponding author. Tel.: +39 0817682198
E-mail address: wmauro@unina.it

capacities but also introduce complex interactions between refrigerant-side two-phase flow and air-side heat and mass transfer.

A critical operational issue for air-source heat pumps in cold and humid climates is frost formation on the evaporator coil surface. Frost accumulation leads to a progressive reduction of the heat transfer coefficient and air flow rate, causing a significant drop in heating capacity. To get back to the nominal performance, defrosting cycles must be operated, typically through hot-gas bypass or hot fluid secondary loops. In large-scale installations, where tens or even hundreds of evaporators operate in parallel, defrosting must be performed in a rational way to ensure uninterrupted service to the district heating network. Consequently, frost formation and defrosting cycles have a direct impact on seasonal performance and must be carefully considered in the design and control of such systems.

The scientific literature provides several analyses on frost formation mechanisms, mainly focused on small and medium-size heat pumps. Several studies have investigated the physics of frost growth on flat or finned surfaces, providing experimental and theoretical benchmarks still widely adopted. The works of Tao et al. (1993) [3] and Lee et al. (1997) [4] developed mathematical models describing frost densification, growth kinetics, and the evolution of frost-layer thermal properties under forced convection. Na and Webb (2004) [5] extended these approaches by proposing a new generalized correlation for frost growth rate, which has become a common reference for the development of dynamic models. More recent works such as Li and Wang (2021) [6] reviewed, compared and unified numerous predictive models for frost formation on plain surfaces, highlighting the influence of environmental conditions such as humidity gradient, surface temperature and airflow rate. Several detailed modelling studies have focused on dynamic simulations of frosting and defrosting cycles for single evaporators. Ma et al. (2023) [7] proposed a high-resolution dynamic modelling framework accounting for both frost growth and reverse-cycle defrosting, validated experimentally but limited to short-time operation windows. Bai et al. (2023) [8] investigated frosting behavior on an innovative novel dual-fan coils geometry, showing how geometric features strongly influence the time evolution of frost resistance and air-side pressure drop. These contributions provide valuable insight into local frosting phenomena but remain limited to isolated components.

Other authors have applied simplified approaches, such as seasonal performance models relying on empirical frost-penalty factors or operating maps. Bagarella et al. (2016) [9] developed a dynamic seasonal simulation including an average frost thickness correlation to trigger electric defrosting cycles, while Milev et al. (2023) [10] showed that the number of required defrost cycles increases sharply when the mean ambient temperature decreases, especially when simplified correlations are used. Liu et al. (2022) [11] proposed condensing-frosting performance maps for variable-speed heat pumps, offering averaged performance indicators but lacking the capability to reproduce complex interactions within multi-evaporator fields.

Recent reviews, such as that by Song et al. (2018) [12], emphasize that while extensive research exists on single-coil systems, large air-source heat pumps present unique challenges. In particular, the presence of many evaporators operating in parallel, each with different frosting histories, introduces strong non-uniformities in airflow distribution, frost accumulation rate, and defrosting needs. On this regard, there is currently a clear gap in the literature regarding physically detailed dynamic models capable of capturing the behavior of entire evaporator fields with alternating defrosting cycles. Existing works either neglect the problem or treat it through simplified correlations that may significantly misrepresent the seasonal efficiency.

To overcome this gap, the present study introduces a new dynamic modelling for the seasonal performance assessment of large air-source heat pumps designed for district heating applications. The main novelty is the detailed representation of each evaporator within the field, allowing independent simulation of frosting and defrosting dynamics as well as their mutual influence on the overall system operation. This approach enables a more accurate estimation of the seasonal energy consumption and provides a tool for identifying thermo-economic optimal configurations in terms of field geometry and defrosting strategy.

The paper is organized as follows. Section 2 describes the heat pump architecture and the evaporator field. Section 3 presents the dynamic modelling framework for frosting and defrosting, whereas Section 4 illustrates the system-level integration and the seasonal simulation methodology. Finally, Sections 5 and 6 discuss the results and provide the main outcome of this work.

2. Large size air-source ammonia heat pump system

A two-stage compression thermodynamic cycle with a wet direct expansion is the architecture of the large size ammonia heat pump considered in this work. A multi-evaporator system made by parallel fin and tube heat exchangers realizes air-refrigerant heat transfer. A hot gas bypass system is involved for defrosting operations. The system scheme is shown in figure 1(a) with the related temperature-specific entropy thermodynamic chart. The thermodynamic assumptions and main equations are detailed reported in previous work as well as the definition of the district heating network demand $\dot{Q}_{DHN}$ during the heating season [13]. The power consumption from low- and high-pressure compressors ($\dot{L}_{C1}$ and $\dot{L}_{C2}$ respectively) consider the eventual defrosting operation as follows:

$$\dot{L}_{C1} + \dot{L}_{C2} = \left(\dot{m}_{int} + \dot{m}_{hgbp}\right) \cdot (h_2 - h_1) + \left(\dot{m}_{co} + \dot{m}_{hgbp}\right) \cdot (h_4 - h_3) \tag{1}$$

Considering also the auxiliary components consumptions $\dot{L}_{aux}$ (i.e. recirculating pumps and axial fans of the evaporator field), the COP is defined as follows:

$$COP = \frac{\dot{Q}_{DHN}}{\dot{L}_{C1} + \dot{L}_{C2} + \dot{L}_{aux}} \tag{2}$$

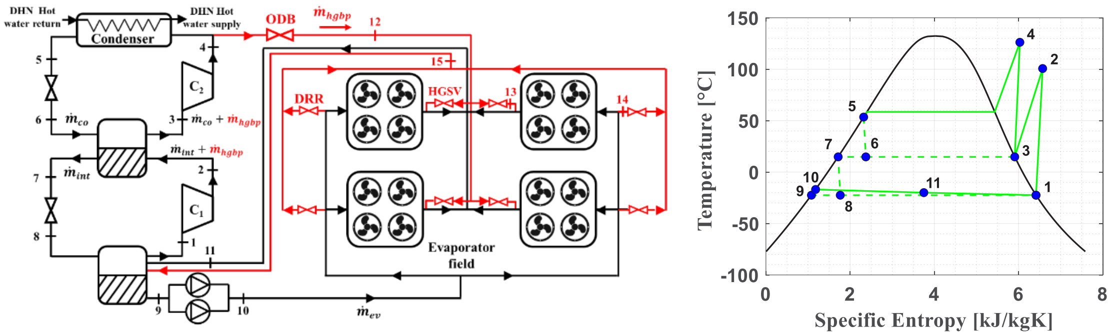

(a) (b)

Figure 1. (a) Schematization of the large size ammonia heat pump modelled with hot gas bypass system [13] and (b) its thermodynamic cycle on the temperature-specific entropy chart.

3. Evaporator field modelling

Each evaporator of the field, as depicted in figure 2, can be characterized by an overall conductance $(UA)_n$ that is affected by two possible operating conditions: free surface or frost formation. In case of defrosting, some evaporators are not providing cooling capacity, having a fraction of the total number of evaporators that are considered operating ($N_{ev,act}$). The active part of the field defines the global conductance UA_{field}, having the field cooling capacity $\dot{Q}_{ev}$. The operating evaporation temperature is the one that satisfies the cooling capacity defined by the heat transfer modelling of the evaporator field and the thermodynamic cycles as expressed in Eqs. (3).

$$\begin{cases} \dot{Q}_{ev} = UA_{field} \Delta T_{air-ref} \\ UA_{field} = \sum_{n=1}^{Nev_{act}} (UA)_n \\ \dot{Q}_{ev} = \dot{m}_{ev} \Delta h_{lv} x_{11} \end{cases} \tag{3}$$

3.1. Evaporator modelling with frost formation

To achieve detailed modelling of the heat exchanger, the single fin-and-tube evaporator of the field (figure 2) is analysed using the "tube-element" approach. This modelling technique discretizes the fin-and-tube coil into multiple elements, allowing for separate energy balance calculations to be performed on both the air and refrigerant sides of every section. All the details regarding the heat transfer evaluation are provided in the previous work [13]. The cooling capacity of the single evaporator is evaluated through the sum of the elementary contributions of the elements dividing the refrigerant circuit multiplied by the number of parallel circuits N_c constituting the fin and tube coil (neglecting uneven distribution on the refrigerant side due to the use of a wet direct expansion system).

$$\dot{Q}_{ev} = N_c \sum_k \dot{Q}_{ref,k} \tag{4}$$

Whenever the surface temperature of the heat exchanger element is both below the dew point of moist air and 0°C a frost formation transient is considered. The growth and densification of the elementary frost thickness is defined by the application of the Hermes et al. approach [14] to divide the total frost mass flux G_f in the growth and densification contributions, named G_g and G_d respectively.

$$G_f = G_g + G_d = K_m(\omega_{air} - \omega_{surface}) \tag{5}$$

The actual air flow rate is determined by finding the operating point where the air-side pressure drop across the evaporator equals the pressure provided by the axial fan's characteristic curve.

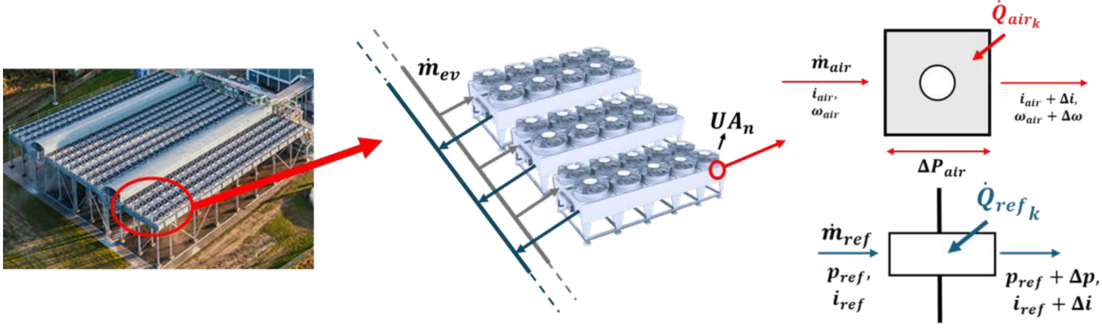

Figure 2. Schematization of the tube element approach for a multi-evaporator system

4. Case study description and simulation plan

4.1. Case study

In this work, an evaporator field linked to a 7 MW heat pump that serves a district heating network located in Harbin (China), providing hot water at 60 °C with a 30 °C return temperature, is investigated. The selected location is characterized by a continental climate which features very low average winter temperatures (-13 °C) and consequently low average specific and relative humidity (about 60%) as described in figure 3. Although weather conditions of this kind are unfavourable for the performance of an air source heat pump, open available water sources could be useless due to freezing issues, thereby supporting the use of this kind of heat pump. Furthermore, the dry climate means that the potential for frost formation is less severe than in climates with higher average temperatures but higher humidity.

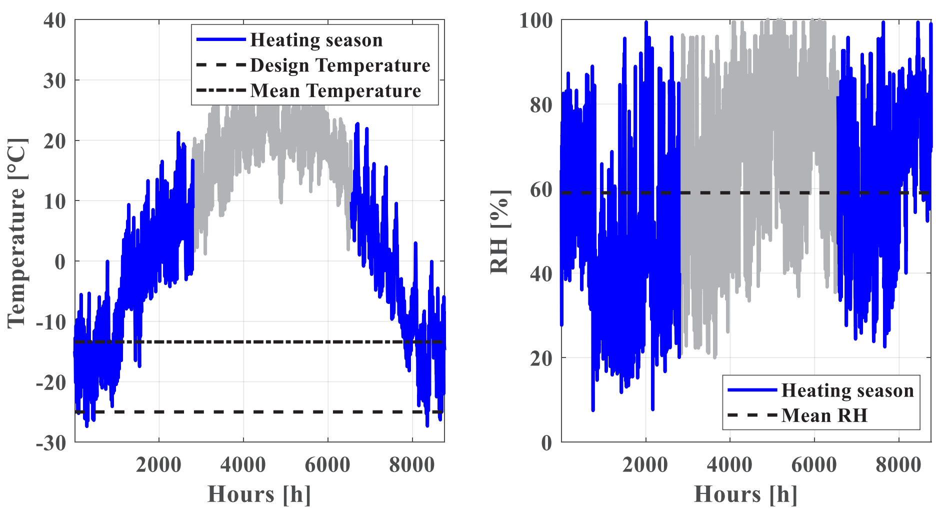

Figure 3. Harbin climatic conditions (data taken from The Joint Research Centre: EU Science Hub - PVGIS)

4.2. Seasonal simulation domain

The design of the evaporator field involves the appropriate definition of the total surface area and heat exchange performance. Combining all geometrical features of a fin-and-tube heat exchangers, the number of evaporators, and the axial fan characteristics, a potential design domain of millions of configurations is obtained. However, considering also the influence of design variables on frost formation intensity, it is possible to obtain a subset of key design variables composed as follows: number of evaporators, nominal airflow velocity, fin pitch and fin type. Considering a domain spanning from 60 to 120 evaporators, 1.5 to 4.5 m/s airflow nominal velocity and 6 to 12 mm fin pitch for both wavy and louvered type, hundreds of configurations can be defined. However, the high computational time required for detailed seasonal simulations prevents the exploration of this entire domain. Therefore, following the same approach applied in another case study [13], a group of convenient thermo-economic solutions in terms of total costs in design conditions, is extracted from the mentioned domain. In particular, 20 configurations, whose characteristics are resumed in table 1, have been selected.

The sum of total energy consumption E_{cons} and the field investment cost C_{field} (provided by the manufacturer) defines total costs C_{tot}. The specific cost of energy is a reference fixed value for the selected location and the running period y considered is equal to 10 years.

$$C_{tot} = E_{cons} \cdot C_{en} \cdot y + C_{field} \quad (6)$$

The integration during the heating season of the instantaneous COP defined in Eq. (2) defines the seasonal coefficient of performance (SCOP). Therefore, total energy consumption is defined by the ratio of the total heating demand of the district heating network E_{DHN} and the SCOP.

$$E_{cons} = \frac{E_{DHN}}{SCOP} \quad (7)$$

Given the zero direct environmental impact of ammonia (GWP = 0), SCOP becomes representative of the environmental impact of the system.

Table 1. Selected design configurations for seasonal simulation assessment

Fin type	Airflow velocity [m/s]	Fin pitch	Evaporator field size
Louvered	1.5	6	60-80-100
		9	80-100
	2.5	9	60-80-100
		12	60-80-100-120
Wavy	2.5	6	60
		9	60-80-100-120
		12	80-100-120

The selected configurations of table 1 are analysed through seasonal simulations. The defrosting strategy implemented is temperature-time based. The trigger time to start defrosting is defined from reference frosting transient simulations for a single evaporator in a critical combination of heating demand by the network and ambient air conditions. The average time for all selected configurations required to reach a cooling capacity decay of -30% and -60% with respect to frost-free evaporator is used as trigger time. For this case study 20 and 40 hours are used.

Furthermore, to not interrupt the service to the network, the number of evaporators to be defrosted simultaneously is equal to fraction of 10% or 20% of the field. A proper time-shifting of trigger defrosting time is assumed when all evaporators start frosting simultaneously after a frost-free operating period.

The permutation of the selected field configurations and the defrosting strategy settings leads to a total plan of 80 seasonal simulations that have been executed in MATLAB using parallel computing techniques for the evaporator field.

5. Results

The best and worst cases resulting from the seasonal simulation domain are described in table 2. The relative comparison between the simulations is shown as the percentage difference in total costs compared to those relating to the best solution $\Delta C_{tot,\%}$. A wavy fin type with 9 mm pitch, 60 evaporators and a nominal airflow velocity of 2.5 m/s characterize the best case. Instead, the worst configuration presents a louvered 6 mm fin pitch, 100 evaporators with a nominal airflow velocity of 1.5 m/s. The maximum difference between the best and worst solutions is of approximately 16%, with an average value of around 5%. In terms of design conditions, the configurations differ by a maximum of 1.5%. The resulting maximum difference is significantly smaller if compared to another case study characterized by a more wet climatic conditions, where the maximum difference was around 70% [13].

The reason for this narrower range is the impact of frost formation and defrosting cycles on seasonal performance. Specifically, the fraction of the heating season spent in conditions favourable to frost formation is equal to 17% for Harbin, a geographic area of low or intermediate frost criticality.

Table 2. Best and worst solutions for the investigated seasonal simulation domain

	Fin type	Airflow velocity [m/s]	Fin pitch	Evaporator field size	Defrosting strategy	$\Delta C_{tot,\%}$ [%]
Best case	Wavy	2.5	9	60	20% - 20h	0.0 %
Worst case	Louvered	1.5	6	100	10% - 20h	16.3 %

Figure 4 shows the overall seasonal simulation results with respect to investigated defrosting strategy settings. Specifically, the best strategy for Harbin is the one involving the least frequent defrosting: defrosting 20% of the field every 40 hours. This finding is supported by a clear downward trend in the 75th percentile value, which decreases from 11.3% to 4.5% as defrosting frequency reduces (even accounting for the effect of design features). For example, the total number of defrosts varies significantly, from approximately 760 in the most frequent combination to approximately 220 in the least frequent one.

Therefore, the least frequent strategy is, on average, the best because of Harbin's low overall need for defrosting. This minimizes the energy and time spent on defrosting without incurring a significant penalty from frost accumulation, leading to lower overall costs.

However, the best case presents a 20%-20h defrosting strategy, suggesting that each geometry has its own optimal combination of defrosting parameters.

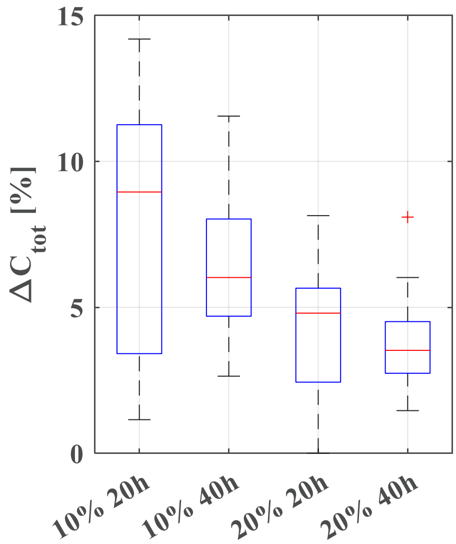

Figure 4. The effect of defrosting strategy settings on total cost percentage difference

Since the investigation of defrosting strategy options is not exhaustive in the search for the optimal combination, the configuration of the design parameters most resilient to the defrosting strategy is analyzed below. In this regard, table 3 presents the average SCOP and total cost increase $\overline{\Delta C_{tot,\%}}$ for each of the 20 configurations (i.e. the average of the four simulations for each configuration resulting from the defrosting strategy permutations). Fins with a pitch of 9 or 12 mm and an airflow velocity of 2.5 m/s are the features of the best configurations. The design features set related to the best case of table 2 are the fourth in terms of average values, but performing better than its counterparts with 80, 100 and 120 evaporators. A higher number of modules, with the other parameters remaining the same, implies a larger total heat exchange surface area, thus offering an advantage in terms of evaporation temperature. This can be seen from the SCOP values without frost formation rising from 3.15 for 60 evaporators to 3.21 for 120 evaporators. However, a higher number of evaporators leads to higher defrosting consumption and, since these defrosting cycles are often unnecessary, the solution with the lowest number of modules is the most cost-effective.

Table 3. Averaged seasonal simulation results for each evaporator field configuration

Fin type	Fin pitch [mm]	Evaporator field size	Airflow velocity [m/s]	SCOP (no frost)	$\overline{SCOP}$	$\overline{\Delta C_{tot,\%}}$ [%]
Louvered	12	80	2.5	3.18	2.90	1.3
Louvered	9	60	2.5	3.15	2.86	2.3
Wavy	12	100	2.5	3.18	2.87	2.4
Wavy	9	60	2.5	3.15	2.85	2.7
Louvered	9	100	2.5	3.22	2.89	3.0
Louvered	12	100	2.5	3.21	2.86	3.5
Louvered	12	60	2.5	3.11	2.81	3.9
Wavy	12	100	2.5	3.19	2.81	5.3
Louvered	12	120	2.5	3.20	2.82	5.6
Wavy	9	100	2.5	3.19	2.79	6.0
Louvered	9	100	1.5	3.22	2.80	6.1
Louvered	9	80	2.5	3.17	2.78	6.2
Wavy	12	120	2.5	3.20	2.80	6.3
Wavy	9	80	2.5	3.18	2.78	6.4
Wavy	9	120	2.5	3.21	2.79	7.2
Louvered	6	80	1.5	3.20	2.77	7.5
Louvered	9	80	1.5	3.19	2.74	7.7
Wavy	6	60	2.5	3.15	2.72	8.5
Louvered	6	100	1.5	3.20	2.74	10.1
Louvered	6	60	1.5	3.17	2.69	10.3

6. Conclusions

This study analyses the seasonal performance of a large air-source heat pump for district heating equipped with a multi-evaporator system installed in Harbin, China. In particular, 80 seasonal simulations were performed by varying both the main characteristics of the evaporator field (number of modules, fin pitch and type, and air velocity) and the main parameters to be set for time-temperature defrosting.

The combination of the effect of geometric parameters and defrosting led to a maximum difference in total costs of approximately 16%. The most cost-effective defrosting strategy, on average, proved to be the one with the least frequent defrosting (20% of the field every 40 hours), showing how predefined time-based defrosting logic can result in unnecessary defrosting for the specific location chosen. Instead, the more convenient design parameters combinations, on average, tend to be characterized by fin pitches of 9 or 12 mm and an air velocity of 2.5 m/s. However, the best solution (9 mm wavy fins, airflow velocity of 2.5 m/s and 60 evaporators) presents the fourth best design parameters combinations and features an intermediate defrost strategy (20% of the field every 20 hours).

Therefore, the main outcome of the study is the following: the average results with respect to a design parameter or a defrosting strategy setting can provide an indication to reach a subdomain of thermo-economic convenience, but it is the combination of effects of both design and defrosting variables that leads to the best seasonal performance, confirming the need for a detailed comprehensive analysis for each case study.

Nomenclature

h	Specific enthalpy [kJ/kg]
Δh_{lv}	Liquid-to-vapor latent heat [kJ/kg]
K_m	Mass transfer coefficient [kg/(m^{2}s)]
$\dot{m}$	Mass flow rate [kg/s]
x	Vapor quality [-]
Greek	
ω	Specific humidity [kg_{H2O}/kg_{air}]

References

[1] IEA. Tracking SDG7, *The energy progress report;* 2025.

[2] IEA. *Net Zero by 2050, A roadmap for the Global Energy Sector;* 2021.

[3] Tao YX, Besant RW, Rezkallah KS, A mathematical model for predicting the densification and growth of frost on a flat place. *Int. J. Heat Mass Transf.* 1993;**36-2:**353-363.

[4] Lee KS, Kim WS, Lee TH. A one-dimensional model for frost formation on a cold flat surface. *Int. J. Heat Mass Transf.* 1997;**40-18**:4359-4365.

[5] Na B, Webb RL. New model for frost growth rate. *Int. J. Heat Mass Transf.* 2004;**47-5**:925-936.

[6] Li SM, Wang CC. Predictive models on the frost formation for plain surface - a review and comparative study. *Int. Commun. Heat Mass Transf.* 2021;**129**:105670.

[7] Ma J, Kim D, Braun JE, Horton WT. Development and validation of a dynamic modeling framework for air-source heat pumps under cycling of frosting and reverse-cycle defrosting. *Energy*. 2023;**272**:127030.

[8] Bai X, Liu X, Deng S, Zhang L, Wei M. A modelling study on the frosting characteristics of a novel dual-fan outdoor coil in an Air Source Heat Pump unit. *Appl. Therm. Eng*. 2023;**222**:119933.

[9] Bagarella G, Lazzarin R, Noro M. Sizing strategy of on–off and modulating heat pump system based on annual energy analysis. *Int. J. Refrig*. 2016; **65** 183-193.

[10] Milev G, Al-Habaibeh A, Fanshawe S, Siena FL. Investigating the effect of the defrost cycles of air-source heat pumps on their electricity demand in residential buildings. *Energy Build*. 2023;**300**:113656.

[11] Liu S, Bai X, Deng S, Zhang L, Wei M. A modeling study on developing the condensing-frosting performance maps for a variable speed air source heat pump. *J. Build. Eng*. 2022;**58**:104990.

[12] Song M, Deng S, Dang C, Mao N, Wang Z. Review on improvement for air source heat pump units during frosting and defrosting. *Appl. Energy*. 2018;**211**:1150-1170.

[13] Passarelli AF, Merlo U, Pelella F, Viscito L, Filippini S, Mauro AW. Air-source ammonia heat pump for district heating: a field modeling approach with focus on frosting-defrosting cycles. *Appl. Th. Eng*. 2026;**282**:128790.

[14] Hermes CJL, Piucco RO, Barbosa JR, Melo C. A study of frost growth and densification on flat surfaces. *Exp. Therm. Fluid Sci*. 2009;**33-2**:371-379.